Journal of Solid State Chemistry **145,** 116–127 (1999)
Article ID jssc.1999.8230, available online at http://www.idealibrary.com on IDEAL®

The $A_{n+2}B_nB'O_{3n+3}$ Family ($B = B' = Co$): Ordered Intergrowth between 2H–$BaCoO_3$ and $Ca_3Co_2O_6$ Structures

K. Boulahya, M. Parras, and J. M. González-Calbet[1]

Departamento de Química Inorgánica, Facultad de Químicas, Universidad Complutense, 28040-Madrid, Spain

Received December 7, 1998; in revised form February 12, 1999; accepted February 18, 1999

The n integer members of the $A_{n+2}B_nB'O_{3n+3}$ homologous series keeping $B = B' = Co$ the same have been characterized by selected area electron diffraction and high resolution electron microscopy. Its commensurate modulated structure is made up of chains, separated by A atoms, running along the c direction containing a succession of one Co atom (B') in prismatic trigonal sites and n Co atoms octahedrally coordinated sharing faces. All of them can be described as ordered intergrowths of two structures of the end members of the family, 2H–$BaCoO_3$ ($n = \infty$) and $Ca_3Co_2O_6$ ($n = 1$). The modulation observed in all terms can be described as a function of the difference between the c-axis of the Co sublattice with respect to the 2H structure. Members of the series can be obtained by modifying the distance between layers keeping $B = Co$ the same, as shown in $(Sr_{1-x}Ba_x)_6Co_5O_{15}$ ($n = 4$), $Sr_5Co_4O_{12}$ ($n = 3$), and $(Sr_{0.5}Ca_{0.5})_4Co_3O_9$ ($n = 2$). © 1999 Academic Press

Key Words: **$A_{n+2}B_nB'O_{3n+3}$ homologous series; 2H related perovskite; Sr_4PtO_6 structural type; electron diffraction; high resolution electron microscopy.**

INTRODUCTION

The striking similarity between two structural types is a way solids can accommodate compositional variations since intermediate compositions can exist with a structure which derives from the limiting structures. This is the case, for instance, in cubic packed anion-deficient perovskites where the close analogy (1) between $A_2B_2O_5$ brownmillerite (2), made up of an ordered sequence of alternating octahedral and tetrahedral layers, and ABO_3 perovskite (3), consisting only of octahedra, allows intermediate compositions $A_nB_nO_{3n-1}$ leading to an ordered intergrowth of $(n-1)$ octahedral layers and one tetrahedral layer (4, 5).

In a similar way, Darriet and Subramanian (6) have established the structural relationships between the 2H-ABO_3 hexagonal perovskite type (7) and the Sr_4PtO_6 type structure (8). The 2H is formed by a hexagonal stacking of A_3O_9 layers with the B cations occupying octahedral sites. The structure can be described as chains of $[BO_6]$ octahedra sharing faces running parallel to the c-axis (Fig. 1a). The Sr_4PtO_6 structure can be also described by the same hexagonal stacking now constituted by $A_3A'O_6$ ($A = A' = Sr$) layers, the chain of polyhedra being formed by the alternance of one PtO_6 octahedron linked by common faces to a triangular prism occupied by strontium atoms (Fig. 1b). On the basis of the hexagonal stacking of mixed A_3O_9 and $A_3A'O_6$ layers, Darriet and Subramanian postulated the existence of a homologous series of general formula $A_{3n+3}A'_nB_{n+3}O_{6n+9}$, n being the number of successive $A_3A'O_6$ layers. The lower limit of this series ($n = 0$) is the 2H–ABO_3 phase while the upper limit ($n = \infty$) is the Sr_4PtO_6 phase. The structure of intermediate terms is made up of chains parallel to the stacking axis separated by A atoms and formed by trigonal prismatic sites occupied by A' cations separated by octahedra sharing faces. Therefore, $Ba_6Ni_5O_{15}$ (9) constitutes the $n = 1$ term of this series where the stacking sequence corresponds to one $A_3A'O_6$ ($A = Ba$; $A' = Ni$) layer and one A_3O_9 layer (Fig. 1c). The $n = 2$ member is $Sr_4Ni_3O_9$ (10) formed by three $A_3A'O_6$ layers and one A_3O_9 layer.

In a recent paper (11), we reported two new compounds which can also be derived from the structural analogy between the hexagonal 2H–$BaNiO_3$ type and the $Ba_6Ni_5O_{15}$ structure: $Ba_9Co_8O_{24}$ and $Ba_8Co_7O_{21}$. However, according to the composition expressed by the above general formula, phases with $B/A > 0.83$ are not included, since this family is limited to compositions in which only single A_3O_9 layers are inserted every n $A_3A'O_6$ layers. All these oxides, however, can be considered as members of a family with the general formula $A_{n+2}B_nB'O_{3n+3}$ where the upper and lower limits are now $n = \infty$ (2H–ABO_3) and $n = 1$ (Sr_4PtO_6), respectively. This general formulation is only valid for a ratio prism/octahedra $= 1/n$, n being an integer.

Very recently, Blake *et al.* (12) proposed a more general classification scheme including members with n no integer, since they have isolated new phases in the

[1] To whom correspondence should be addressed.

0022-4596/99 $30.00

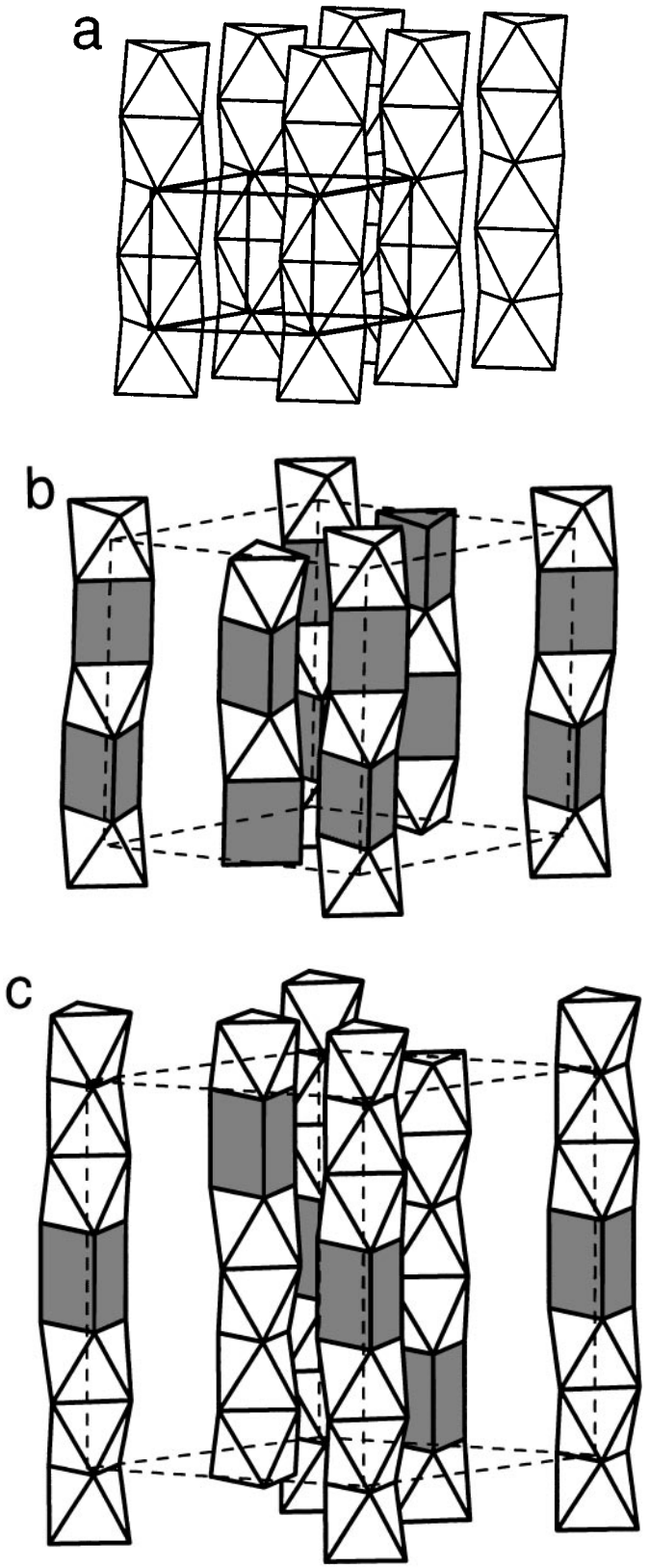

FIG. 1. Ideal structures of (a) 2H–ABO_3; (b) $Ca_3Co_2O_6$, and (c) $A_6B_5O_{15}$.

barium–copper–iridium–oxygen system with one or more prismatic sites per row per unit cell. On the basis of the relationship between layers (either A_3O_9 or $A_3A'O_6$) and polyhedra per unit cell, they predict new commensurate structures while allowing for the incommensurate nature of materials in this family.

In this paper, we summarize all the n integer terms up to now isolated in the homologous series $A_{n+2}B_nB'O_{3n+3}$ when $A' = B = Co$. $BaCoO_3$ (13) adopts the 2H structural type and constitutes the $n = \infty$ term, while $Ca_3Co_2O_6$ (14), isostructural to Sr_4PtO_6, is the $n = 1$ member. Besides, $Ba_9Co_8O_{24}$ and $Ba_8Co_7O_{21}$ constitute the $n = 7$ and 6 terms, respectively (11). Attempts to isolate the $Ba_6Co_5O_{15}$ phase have not been successful, although the $n = 4$ term is stable for $Sr_6Co_5O_{15}$ (15). This suggested that in order to stabilize $n \leq 5$ terms of this series it is necessary to decrease the distance between AO_3 layers by reducing the size of the cations in A positions. In this way, the $n = 5$ term of the previous family was isolated for $(Sr_{0.5}Ba_{0.5})_7Co_6O_{18}$ (11). Moreover, Christoffersen *et al.* (16) have characterized by TEM the nonstoichiometric oxide $Sr_5Co_4O_{12-x}$, based on a 3/2 ratio of mixed Sr_3CoO_6 and Sr_3O_9 layers, which should constitute the $n = 1.5$ term of the family $A_{3n+3}A'_nB_{n+3}O_{6n+9}$ or the $n = 3$ member of the series $A_{n+2}B_nB'O_{3n+3}$. It seems clear that the progressive decrease of the distance between AO_3 layers by partial introduction of Sr and Ca lead to lower members of this series. We report in this paper the integer terms of the $A_{n+2}B_nB'O_{3n+3}$ family which can be stabilized with Co occupying both octahedral and prismatic sites, by varying the nature and proportion of the alkaline-earth cation. The structural relationships which can be established between these members and the 2H-structural type are described, from selected area electron diffraction (SAED) and high resolution electron microscopy (HREM) data, in terms of commensurate modulated structures.

EXPERIMENTAL

$(Sr_xBa_{1-x})_6Co_5O_{15}$ was prepared by heating in air stoichiometric amounts of $BaCO_3$, $SrCO_3$, and Co_3O_4 at 875°C for 4 days. $(Sr_xCa_{1-x})_5Co_4O_{12}$ and $(Sr_{0.5}Ca_{0.5})_4Co_3O_9$ were prepared by heating in air at 800°C stoichiometric amounts of $SrCO_3$, $CaCO_3$, and Co_3O_4 for 6 and 3 days, respectively. In order to compare the more streaking microstructural characteristics, $Ca_3Co_2O_6$ was also prepared as described in Ref. (14). The average cationic composition was established by inductive coupling plasma. The local composition in every crystal was determined by energy dispersive spectroscopy (EDS) on a JEOL scanning electron microscope JSM-8600 equipped with an energy-dispersive system LINK AN10000. All results are consistent with the nominal compositions. The oxygen content was determined, within $\pm 1.10^{-2}$, from the average oxidation

state of cobalt analyzed by titration using Mohr's salt. The Co average oxidation state is, in all cases, very close to $(4z-2)/z$, z being the number of Co atoms per unit formula.

Powder X-ray diffraction was performed on a Philips X'Pert diffractometer using Cu$K\alpha$ radiation. SAED was carried out on a JEOL 2000FX electron microscope, fitted with a double tilting goniometer stage ($\pm 45°$). HREM was carried out on a JEOL 4000EX electron microscope, fitted with a double tilting goniometer stage ($\pm 25°$), by working at 400 Kv. Samples were dispersed in *n*-butanol and transferred to carbon-coated copper grids.

RESULTS AND DISCUSSION

Figure 2 shows the powder X-ray diffraction patterns corresponding to $(Sr_{0.75}Ba_{0.25})_6Co_5O_{15}$, $Sr_5Co_4O_{12}$, $(Sr_{0.5}Ca_{0.5})_4Co_3O_9$, and $Ca_3Co_2O_6$, which will subsequently be called (6:5), (5:4), (4:3), and (3:2) phases, respectively. As it can be observed, all patterns show similar characteristics, since these oxides exhibit either trigonal or rombohedral cells with an a parameter close to 1.0 nm and differ from one another by the value of the c parameter, which corresponds to the stacking direction of the octahedra and prisms.

The first one is isostructural to $Sr_6Co_5O_{15}$ (15) with rhombohedral symmetry and parameters of $a = 0.958$ nm and $c = 1.249$ nm. No extra diffraction maxima were observed. By increasing the Ba amount, a mixture of phases is obtained, suggesting that the stability range of the solid solution $(Sr_{1-x}Ba_x)_6Co_5O_{15}$ is $0 \le x \le 0.25$; the unit cell parameters increase as the Ba amount increases due to the higher size of Ba^{2+} (17). $Sr_5Co_4O_{12}$ shows a single phase diffraction pattern which can be indexed on the basis of a trigonal cell with parameters $a = 0.94$ nm and $c = 2.02$ nm. When Sr is partially substituted by Ca, the solid solution $(Sr_{1-x}Ca_x)_5Co_4O_{12}$ is obtained which is stable in the range $0 \le x \le 0.33$, the c-axis decreases as x increases due to the lower ionic radius of Ca^{2+} (13). The phase (4:3)

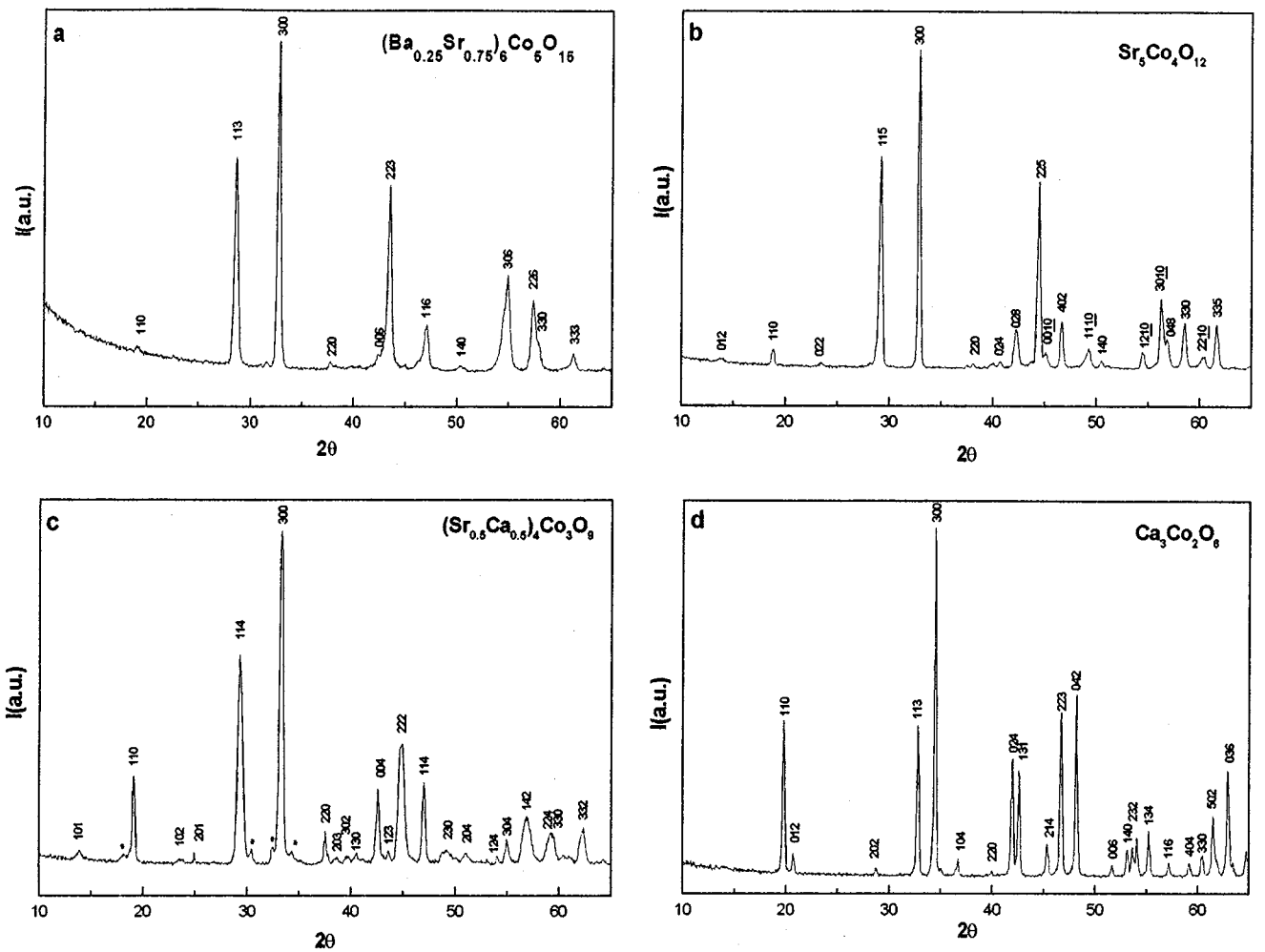

FIG. 2. Powder X-ray diffraction patterns corresponding to (a) $(Sr_{0.75}Ba_{0.25})_6Co_5O_{15}$, (b) $Sr_5Co_4O_{12}$, (c) $(Sr_{0.5}Ca_{0.5})_4Co_3O_9$ (weak maxima marked with $*$ correspond to the (9:7) phase) (14), and (d) $Ca_3Co_2O_6$.

shows diffraction maxima corresponding to a trigonal cell (SG: P321), with parameters $a = 0.928$ nm and $c = 0.806$ nm, and is isostructural to $Sr_4Ni_3O_9$, recently isolated by Huvé *et al.* (10), constituted by chains of two NiO_6 octahedra separated by strontium ions and one Ni face-sharing trigonal prism. The phase (3:2) can be indexed, according to Fjellvag *et al.* (14), on the basis of a rhombohedral cell, SG: $R\bar{3}c$, and parameters of $a = 0.907$ nm and $c = 1.038$ nm. SAED and HREM were used to elucidate unambiguously the stacking sequence of prisms and octahedra along the *c*-axis.

The SAED pattern corresponding to $(Sr_{0.75}Ba_{0.25})_6Co_5O_{15}$ along $[1\bar{1}00]_{2H}$ is shown in Fig. 3a. A commensurate modulated 6-fold superstructure along the $[22\bar{4}2]^*_{2H}$ direction is observed, as a consequence of the location of the Co atoms in prism coordination in every six $(22\bar{4}2)_{2H}$ planes as in $Ba_6Ni_5O_{15}$ (9), in such a way that they are aligned following the $[\bar{3}\bar{3}63]_{2H}$ direction. The corresponding HREM image (Fig. 3b) shows an apparently well-ordered material with $d_{001} = 1.25$ nm and $d_{100} = 0.83$ nm, in agreement with the unit cell described for $Sr_6Co_5O_{15}$ (15). Both figures are similar to that shown by the isostructural material $Ba_6Ni_5O_{15}$ (9); therefore, the sequence of bright dots of different contrast in the image can be associated to cobalt columns formed by one prism and four octahedra sharing faces along the *c*-axis. The two brightest dots correspond to Co prisms along $[\bar{3}\bar{3}63]_{2H}$. Simulated images, performed with the help of a simulation program using the Mac

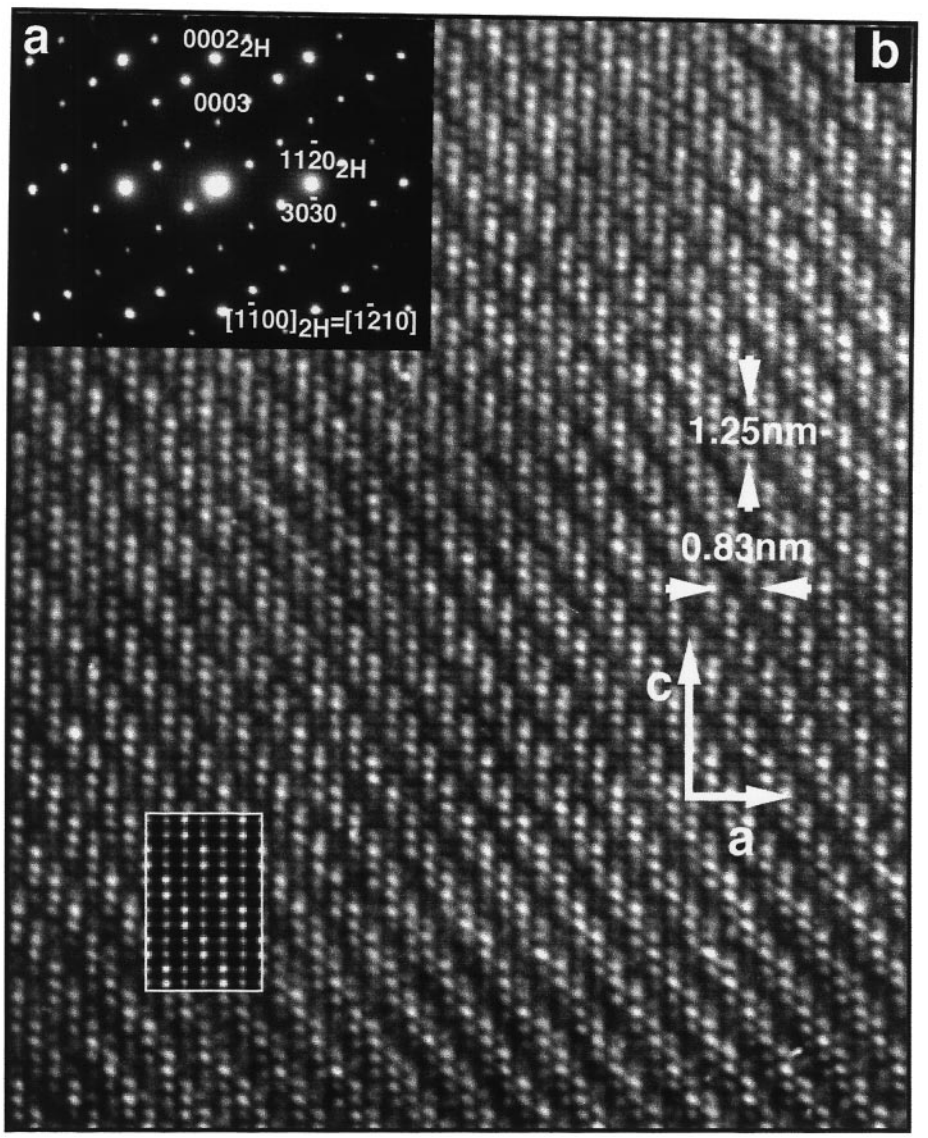

FIG. 3. (a) SAED pattern corresponding to $(Sr_{0.75}Ba_{0.25})_6Co_5O_{15}$ along $[1\bar{1}00]_{2H}$. (b) Corresponding HREM image. The calculated image is shown in the inset.

Tempas package and the atomic positional parameters determined by means of neutron diffraction data by Harrison *et al.* (15), match with the experimental image for $\Delta f = -90$ nm and sample thickness of 5.0 nm.

The most outstanding result given by electron diffraction for this phase in comparison to the structural data obtained either by single crystal X-ray diffraction for $Ba_6Ni_5O_{15}$ or neutron diffraction for $Sr_6Co_5O_{15}$ is in the appearence of a modulation in the intensity of the diffraction spots along the $[22\bar{4}2]^*_{2H}$ direction. The modulation vector k can be expressed, in a general way, as $k = (a^* + b^*)/3 + m2c^*$, a^*, b^*, and c^* referring to the 2H sublattice, m can be obtained by the expression $m = 1/(n + 2)$, where $(n + 2)$ is the number of A atoms per unit cell. Therefore, the m value for the (6:5) phase is 1/6. Such a modulation is a consequence of a nonregular displacement of the atoms in both A and Co sublattices with respect to the ideal positions of the 2H basic subcell. In the 2H type (Fig. 4a), Ba and Co atoms alternate regularly along the c-axis in such a way that Ba atoms are in the $(22\bar{4}2)_{2H}$ planes whereas one of the every two $(44\bar{8}4)_{2H}$ planes are occupied by Co atoms. On the contrary, in the phase (6:5) (Fig. 4b) the rearrangement of Co atoms along the c-axis (placed at $z = 0.095$, 0.299, 0.5), leads to the movement from the same $(44\bar{8}4)_{2H}$ planes to five planes unequidistant, but parallel to the previous ones. On the other hand, the A atoms are also slightly displaced in the (ab) plane; therefore, they are not exactly included in the $(22\bar{4}2)_{2H}$ planes. As a result, a modulation both compositional and displacive takes place along the $[22\bar{4}2]^*_{2H}$ direction, in such a way that if we consider the two metallic subsystems separately, both sublattices should be modulated.

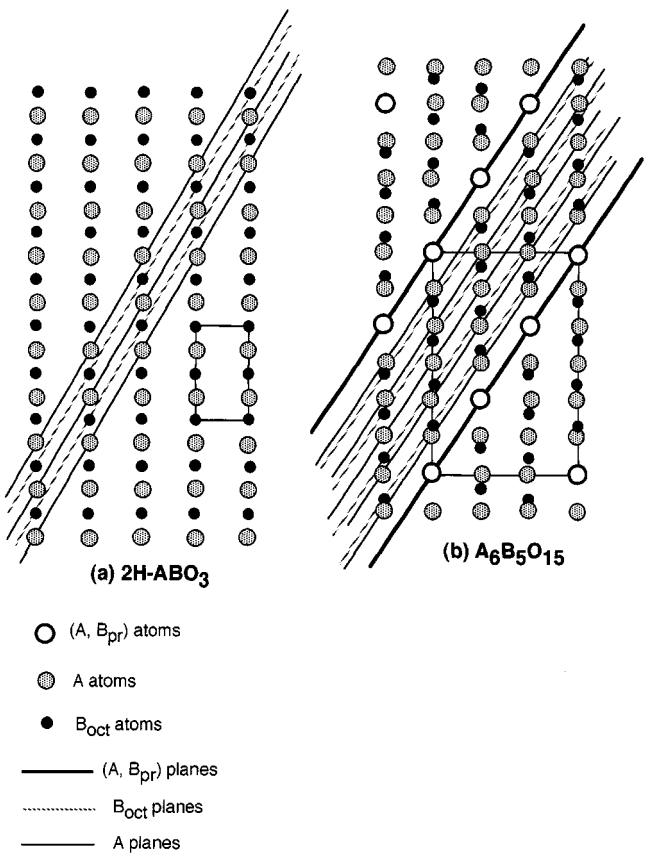

FIG. 4. Schematic representation of (a) 2H and (b) (6:5) structures along $[1\bar{1}00]_{2H}$. The displacement of both A and Co atoms in respect to the 2H type is shown.

The calculated SAED pattern with the previous atomic parameters for the A sublattice shows such a modulation (Fig. 5a). Besides the most intense reflections corresponding to the 2H hexagonal sublattice, first satellite reflections along $[22\bar{4}2]^*_{2H}$ are seen due to the small deviation of A atoms from its ideal positions of the 2H sublattice in the (ab) plane. The calculated electron diffraction pattern corresponding to the Co sublattice is shown in Fig. 5b. Third order satellite reflections are seen along the $[22\bar{4}2]^*_{2H}$ direction. However, the most intense reflections correspond to a rhombohedral lattice instead of hexagonal with a parameter $c^*_{Co} = 5/6(2c^*_{2H})$. If we consider both sublattices independently, c^*_{Co} and $2c^*_{2H}$ (c^*_A) are different, but $6c^*_{Co} = 5(2c^*_{2H})$. The juxtaposition of both patterns leads to the calculated pattern for $(Sr_{0.75}Ba_{0.25})_6Co_5O_{15}$ (Fig. 5c) which is in agreement with the experimental one (see Fig. 3a). Taking into account that the difference between the vectors c^*_{Co} and c^*_{2H} is the c component of vector k, it can also be expressed as $k = (a^* + b^*)/3 + (2c^*_{2H} - c^*_{Co})$.

Figure 6a shows the SAED pattern of $Sr_5Co_4O_{12}$ corresponding to the $[1\bar{1}00]_{2H}$ zone axis. The characteristics of this pattern are analogous to those observed for the (6:5) phase. All crystals observed showed the same diffraction patterns and a Sr:Co ratio equal to 5:4 as characterized by EDS. All diffraction maxima can be indexed on the basis of a three-dimensional unit cell, constituted by ten layers, with parameters $a = b \approx \sqrt{3}a_{2H}$ and $c = 5c_{2H}$ and $P3c1$ space group, since only (0001) reflections with $1 = 2n$ are seen. The HREM image along the $[1\bar{1}00]_{2H}$ zone axis (Fig. 6b) shows an apparently well-ordered crystal with d-spacings 1.01 and 0.84 nm, corresponding to d_{002} and d_{100}, respectively. The contrast variation in the $Sr_5Co_4O_{12}$ image can be interpreted as due to the ordered intergrowth along the c-axis of one trigonal prism and three octahedra sharing faces as a consequence of an ordered stacking sequence of two blocks (Sr_3O_9/Sr_3CoO_6) and one Sr_3CoO_6 layer along the same direction. Following the comparison with the 2H-sublattice, this phase can be considered as a commensurate modulated 15-fold superstructure along the $[55\bar{1}\bar{0}6]^*_{2H}$ direction, in agreement with the situation of Co prisms in three successive $(55\bar{1}\bar{0}6)_{2H}$ planes for every fifteen units. Therefore, the Co prisms are not aligned along the cell diagonal. This misalignment leads to a structure which is no longer rhombohedral. The simulated image corresponding

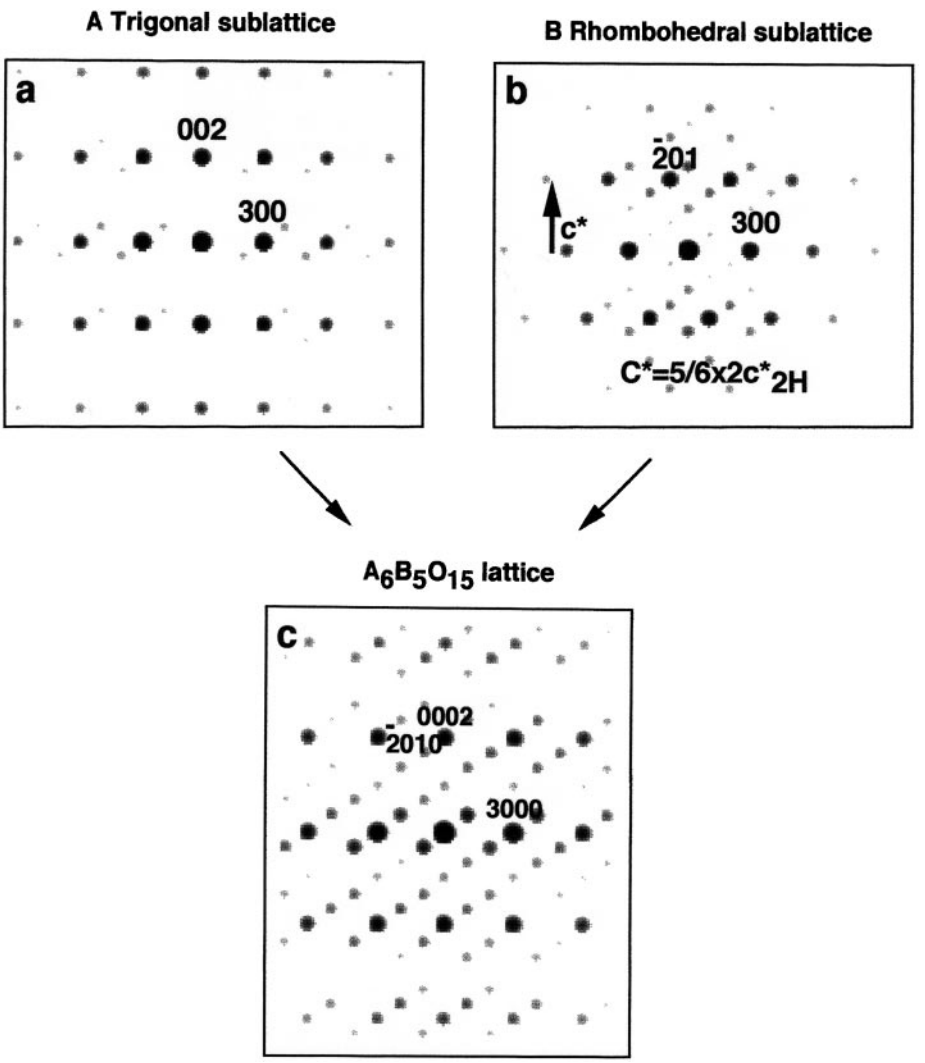

FIG. 5. Calculated SAED patterns along [1$\bar{1}$00] for (a) *A* sublattice in the (6:5) phase; (b) *B* sublattice in the (6:5) phase; (c) $A_6B_5O_{15}$.

to $Sr_5Co_4O_{12}$ along $[1\bar{1}00]_{2H}$ has been calculated on the basis of the model we propose, according to the *P*3*c*1 space group and the ideal atomic positions gathered in Table 1. A good fit with the experimental image is obtained for $\Delta f = -90.0$ nm and a sample thickness of 7.0 nm. The ideal structural model corresponding to the (5:4) phase is shown in Fig. 6c.

It is worth emphasizing that Christoffersen *et al.* (16) show two different diffraction patterns for crystals with the nominal composition $Sr_5Co_4O_{12-x}$. The first one (Fig. 1c in Ref. (16)), which is a single crystal slow-cooled in pure O_2, corresponds to the [100] zone axis of the (5:4) phase. However, the second one (Fig. 2a in Ref. (16)), which is a single crystal grown from molten KOH flux and has also been indexed along the [100] zone axis of incommensurate $Sr_5Co_4O_{12-x}$, corresponds, in fact, to the same reciprocal plane of a crystal showing a close cationic composition but slightly different: $Sr_{14}Co_{11}O_{33}$. As it can be observed in Fig. 6d, this is another commensurate phase due to the ordered intergrowth of one (5:4) and one (4:3) unit cell along the *c*-axis. This stacking sequence has also been reported for Blake *et al.* (12) for the composition $Ba_{14}Cu_3Ir_8O_{33}$ (7 layers ($p = 7$) and 11 polyhedra ($q = 11$) per unit cell).

Figure 7a shows the SAED pattern corresponding to $(Sr_{0.5}Ca_{0.5})_4Co_3O_9$ along $[1\bar{1}00]_{2H}$. Besides the most intense maxima corresponding to $(11\bar{2}0)$ and (0002) of the 2H sublattice, a 12-fold commensurate modulated superstructure along $[44\bar{8}6]^*_{2H}$ is apparent, resulting in a 3-fold superstructure along $[11\bar{2}0]^*_{2H}$ and a two-fold superstructure along c^*_{2H}. All diffraction maxima can be indexed on the basis of a trigonal unit cell, constituted by four layers, with

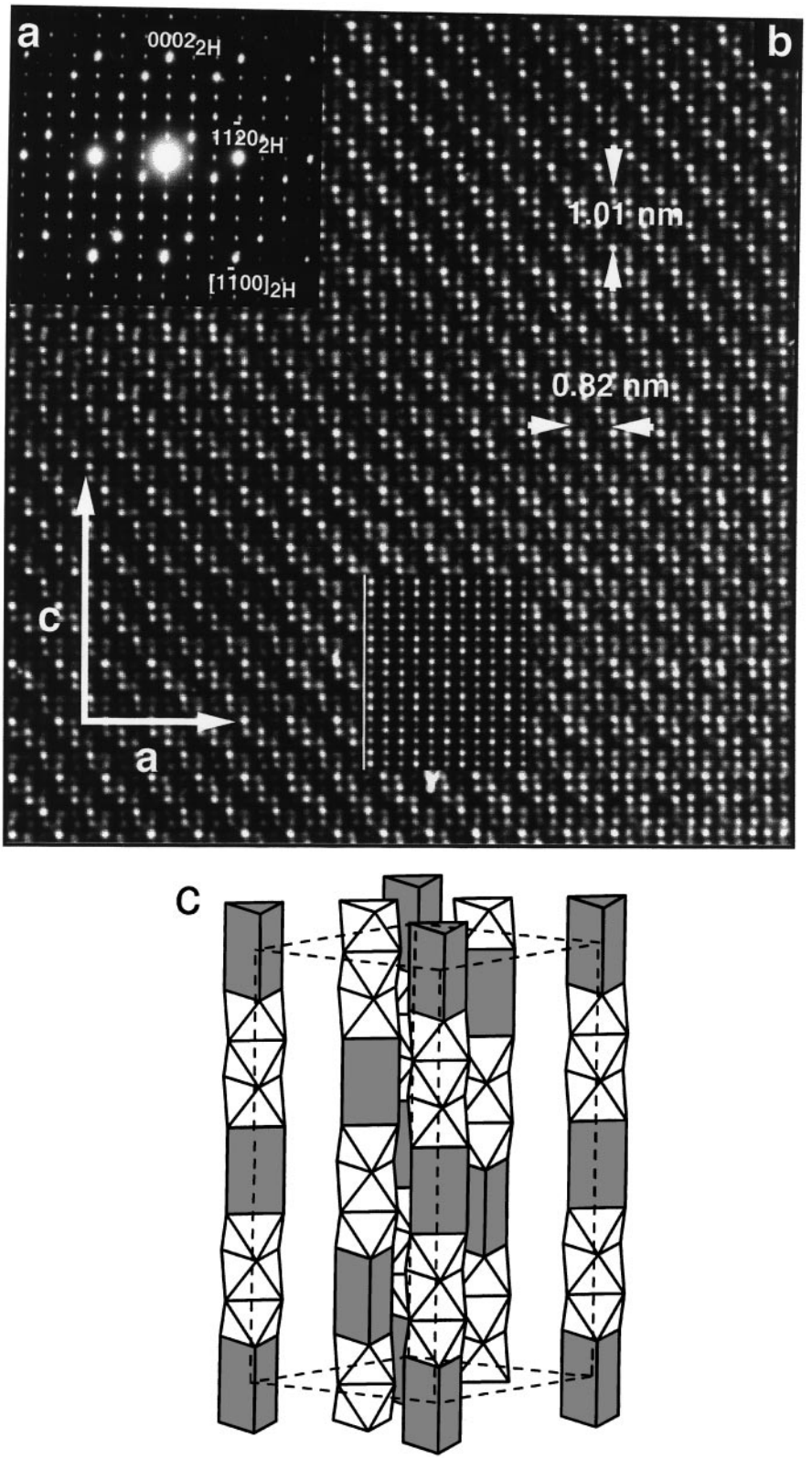

FIG. 6. (a) SAED pattern of $Sr_5Co_4O_{12}$ corresponding to the $[1\bar{1}00]_{2H}$ zone axis. (b) HREM image along $[1\bar{1}00]_{2H}$. The calculated image is shown at the inset. (c) Structural model. (d) SAED pattern and HREM image corresponding to $Sr_{14}Co_{11}O_{33}$ along $[1\bar{1}00]_{2H}$. The calculated image for $\Delta t = 0.7$ nm and $\Delta f = -0.9$ nm is included. Superstructure direction is indicated by an arrow in the SAED pattern. Unit cell is outlined in the image. The ordered intergrowth of (5:4) and (4:3) frames is shown.

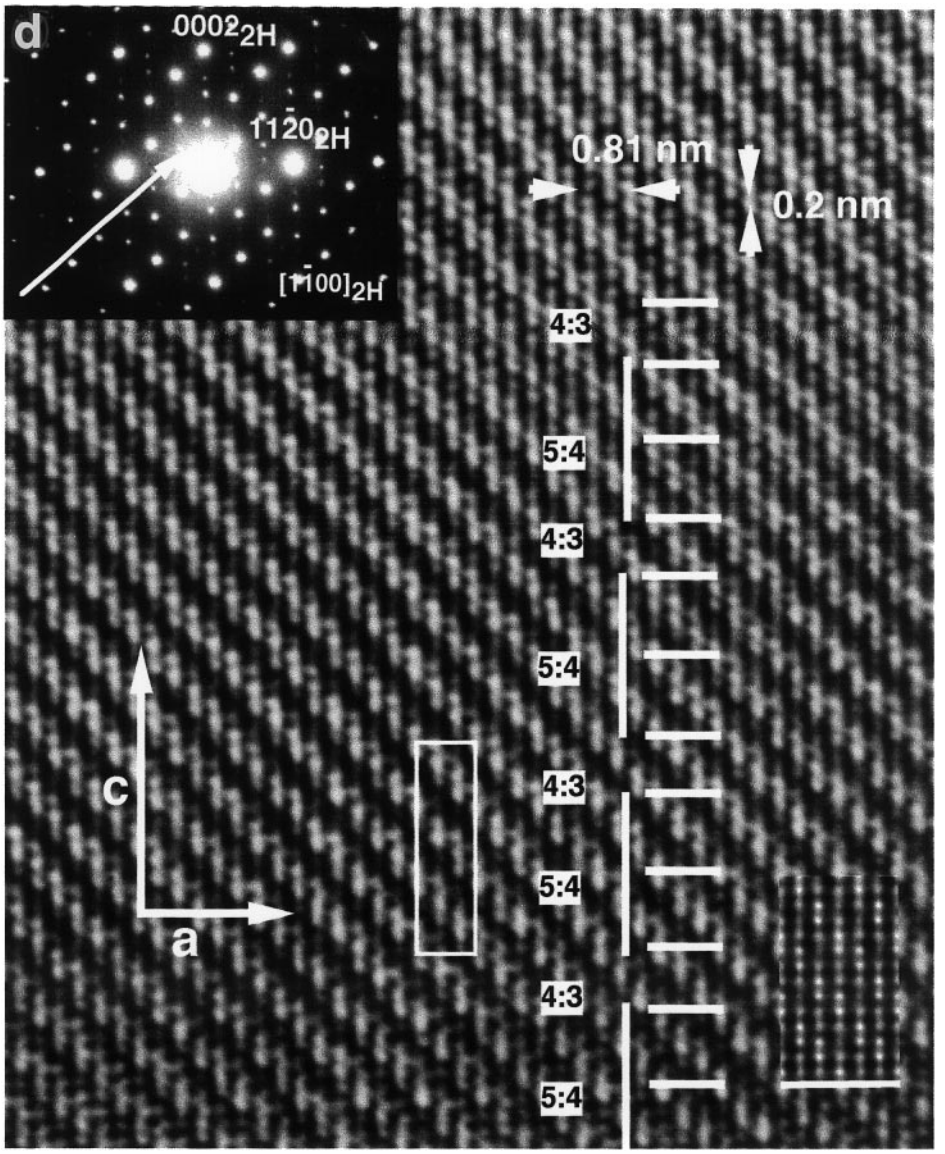

FIG. 6—*Continued*

parameters $a = b = \sqrt{3}a_{2H}$ and $c = 2c_{2H}$. This material, isostructural to $Sr_4Ni_3O_9$ (10), is formed by the ordered hexagonal sequence of one A_3O_9 layer and three A_3CoO_6 layers per unit cell along the *c*-axis, leading to polyhedra rows running parallel to the *c*-axis constituted for one trigonal prism and two octahedra sharing faces. The HREM image along $[1\bar{1}00]_{2H}$ shows an apparently ordered crystal with $d_{001} = 0.806$ nm and $d_{100} = 0.80$ nm (Fig. 7b). The simulated image, calculated on the basis of the $Sr_4Ni_3O_9$ atomic parameters, shows a good fit with the experimental one for $\Delta f = -65.0$ nm and a sample thickness of 7.0 nm. Under the conditions used here, the bright dots observed correspond to columns consisting of cobalt prismatic interstices and of *A* cations.

Figure 8a shows the SAED pattern along $[1\bar{1}00]_{2H}$ corresponding to $Ca_3Co_2O_6$. A three-fold superstructure along $[11\bar{2}2]^*_{2H}$ is observed. All diffraction maxima can be indexed on the basis of a rhombohedral unit cell, with parameters $a = b = \sqrt{3}a_{2H}$ and $c = 3c_{2H}$. This phase is constituted by a hexagonal sequence of six Ca_3CoO_6 layers per unit cell leading to rows of polyhedra running parallel to the *c*-axis formed by one trigonal prism and one octahedra sharing faces. The HREM image along $[1\bar{1}00]_{2H}$ shows an apparently ordered crystal with $d_{002} = 0.54$ nm and $d_{100} = 0.78$ nm (Fig. 8b). Two different areas are seen as a consequence of a difference in the thickness. The simulated image, calculated on the basis of the $Ca_3Co_2O_6$ atomic parameters (14) shows a good fit with the experimental one for

TABLE 1
Ideal Atomic Coordinates for $Sr_5Co_4O_{12}$ (Space group *P*3*c*1)

Atom	Position	*x*	*y*	*z*
Sr1	6*d*	0.666	0.000	0.000
Sr2	6*d*	0.333	0.000	0.100
Sr3	6*d*	0.666	0.000	0.200
Sr4	6*d*	0.333	0.000	0.300
Sr5	6*d*	0.666	0.000	0.400
Co1[a]	2*a*	0.000	0.000	0.000
Co2	2*a*	0.000	0.000	0.250
Co3	2*a*	0.000	0.000	0.150
Co4	2*a*	0.000	0.000	0.350
Co5[a]	2*b*	0.333	0.666	0.400
Co6	2*b*	0.333	0.666	0.500
Co7	2*b*	0.333	0.666	0.15
Co8	2*b*	0.333	0.666	0.250
Co9[a]	2*c*	0.666	0.333	0.2
Co10	2*c*	0.666	0.333	0.35
Co11	2*c*	0.666	0.333	0.05
Co12	2*c*	0.666	0.333	0.45
O1	6*d*	0.500	0.166	0.000
O2	6*d*	0.166	0.500	0.000
O3	6*d*	0.166	0.166	0.100
O4	6*d*	0.666	0.166	0.100
O5	6*d*	0.333	0.500	0.100
O6	6*d*	0.166	0.000	0.200
O7	6*d*	0.166	0.50	0.200
O8	6*d*	0.166	0.166	0.300
O9	6*d*	0.666	0.16	0.300
O10	6*d*	0.333	0.50	0.300
O11	6*d*	0.166	0.000	0.400
O12	6*d*	0.500	0.166	0.400

[a] Cobalt atoms in prismatic coordination.

$\Delta f = -95.0$ nm and a sample thickness of 2.5 nm in the area marked *A* and $\Delta f = -65.0$ nm and a sample thickness of 7.0 nm in area marked *B*. In area *A*, the sequence of bright dots of different contrast can be associated to Co columns formed by one prism and one octahedra. In area *B*, only the contrast associated to Co prisms is apparent.

Figure 9 shows the schematic representation of the projected structural models corresponding to (6 : 5), (5 : 4), (4 : 3), and (3 : 2) phases. The $n = 3$ term is a homogeneous phase formed by the ordered intergrowth along the *c*-axis of one unit cell of the 2H-type ($n = \infty$) and another of the $Ca_3Co_2O_6$ structure ($n = 1$), i.e., the structures limiting this series. The phases (6 : 5) and (4 : 3) are the terms $n = 4$ and 2, respectively, and, as all the members of the $A_{n+2}Co_nCoO_{3n+3}$ series reported until now, can be described as constituted by rows of polyhedra formed by one trigonal prism and *n* octahedra sharing faces running parallel along the *c*-axis, the main difference being the number of octahedra between prisms.

Another common feature in all these terms is the presence of a commensurate modulated superstructure, which can be interpreted in the same way as previously mentioned for the (6 : 5) phase. The superstructure reciprocal direction is $[n + 2,\ n + 2,\ i\ 6]^*_{2H}$, which corresponds to the planes containing the Co atoms in trigonal prisms. The modulation observed in all cases can be associated to the displacement of Ba and Co atoms with respect to the 2H phase positions, the vector modulation being $k = (a^* + b^*)/3 + m2c^*_{2H}$.

On the other hand, such a displacement leads to two metallic sublattices presenting different symmetry and different *c** parameter. The relationship between both reciprocal axes is $2c^*_{2H}/c^*_{Co} = (n + 2)/(n + 1)$, *n* being the number of Co atoms in octahedra per unit cell. Therefore, these phases can be considered as formed by two modulated subsystems (18). The first one corresponds to the Ba sublattice and presents trigonal symmetry and *c* similar to the c_{2H} parameter. The second one corresponds to the Co sublattice with rhombohedral symmetry and a value of the *c* parameter corresponding to c_{Co}. Alternatively, these patterns can be indexed by using a set of four indices *h*, *k*, *l*, and *m*, corresponding to a^*_h, b^*_h, c^*_h, and *c**. The satellite reflections

TABLE 2
Chemical Composition and Crystallographic Data of the Terms Described for the Homologous Series $A_{n+2}B_nB'O_{3n+3}$

Term (*n*)	Composition $A_{n+2}B_nB'O_{3n+3}$	*c*[a] (nm)	Space group	Superstructure direction $[n+2\ n+2\ i\ 6]^*_{2H}$	$k = (a^* + b^*)/3 + m2c^*_{2H}$ (*m*)	$2(n+1)c_{Co} = (n+2)c_{2H}$	Ref.
1	$Ca_3Co_2O_6$	1.038	$R\bar{3}c$	$[3\ 3\ i\ 6]^*_{2H}$	1/3	$4c_{Co} = 3c_{2H}$	14
2	$(Sr_{0.5}Ca_{0.5})_4Co_3O_9$	0.806	*P*321	$[4\ 4\ i\ 6]^*_{2H}$	1/4	$3c_{Co} = 2c_{2H}$	10[b]
3	$Sr_5Co_4O_{12}$	2.02	*P*3*c*1	$[5\ 5\ i\ 6]^*_{2H}$	1/5	$8c_{Co} = 5c_{2H}$	16,[b]
4	$(Ba_{0.25}Sr_{0.75})_6Co_5O_{15}$	1.286	*R*32	$[6\ 6\ i\ 6]^*_{2H}$	1/6	$5c_{Co} = 3c_{2H}$	9, 15,[b]
5	$(Ba_{0.5}Sr_{0.5})_7Co_6O_{18}$	3.02	$P\bar{3}c1$	$[7\ 7\ i\ 6]^*_{2H}$	1/7	$12c_{Co} = 7c_{2H}$	11
6	$Ba_8Co_7O_{21}$	1.75	*P*321	$[8\ 8\ i\ 6]^*_{2H}$	1/8	$7c_{Co} = 4c_{2H}$	11
7	$Ba_9Co_8O_{24}$	3.96	$R\bar{3}c$	$[9\ 9\ i\ 6]^*_{2H}$	1/9	$16c_{Co} = 9c_{2H}$	11
∞	$BaCoO_3$	0.474	$P6_3/mmc$	No superstructure	0	$2c_{Co} = c_{2H}$	13

[a] In all cases, $a = b \approx a_{2H}\sqrt{3}$.
[b] This work.

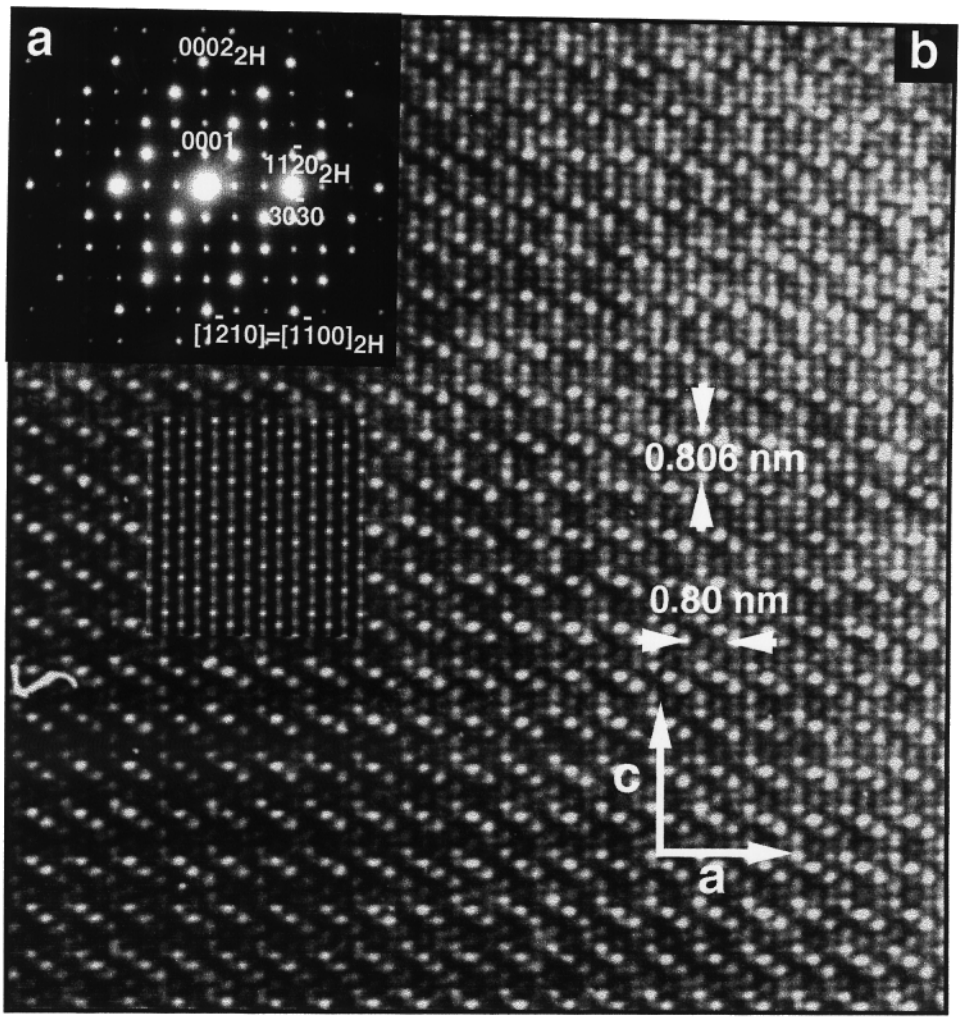

FIG. 7. (a) SAED pattern corresponding to $(Sr_{0.5}Ca_{0.5})_4Co_3O_9$ along $[1\bar{1}00]_{2H}$. (b) Corresponding HREM image. The calculated image is shown at the inset.

are caused by the interaction between both Ba and Co sublattices. It is worth recalling that both descriptions are valid since the z component of the k vector corresponds precisely to the difference between $2c^*_{2H}$ and c^*_{Co}, so k can also be expressed as $k = (a^* + b^*)/3 + (2c^*_{2H} - c^*_{Co})$. In this paper, we have adopted the first description since it is more appropriate to establish the relationship between the 2H type and the different terms of the homologous series.

In Table 2, the different members with n integer up to known found in this system keeping $B =$ Co the same are shown. It is worth mentioning that even keeping only one cation in B sites, a considerable number of homogeneous commensurate phases can be isolated. The difficulty resides in a good selection of the adequate size of the cations occupying A positions for every $A:B$ ratio simultaneously to the synthesis temperature and annealing time.

For $n > 7$, to stabilize the sequence of only one prism separated by n octahedra seems to be complicated. In fact, as we will report in a forthcoming paper, to stabilize higher terms in the experimental conditions used requires the introduction of a higher number of prisms per row, thus leading to members with no integer n values. An example of a noninteger member of this family has been shown in Fig. 6d for $Sr_{14}Co_{11}O_{33}$ which corresponds to the $n = 2.67$ term of the $A_{n+2}B_nB'O_{3n+3}$ series.

All structures can be described by considering only two structural frames in such a way that each one can be built by the addition of one octahedra, i.e., half a unit cell of the 2H-type, per row with respect to the lower term. As a consequence, when n increases in a unit, the c parameter increases $0.5c_{2H}$ times. This increase of the unit cell leads to a variation of the superstructure direction which limits to $[11\bar{2}0]$

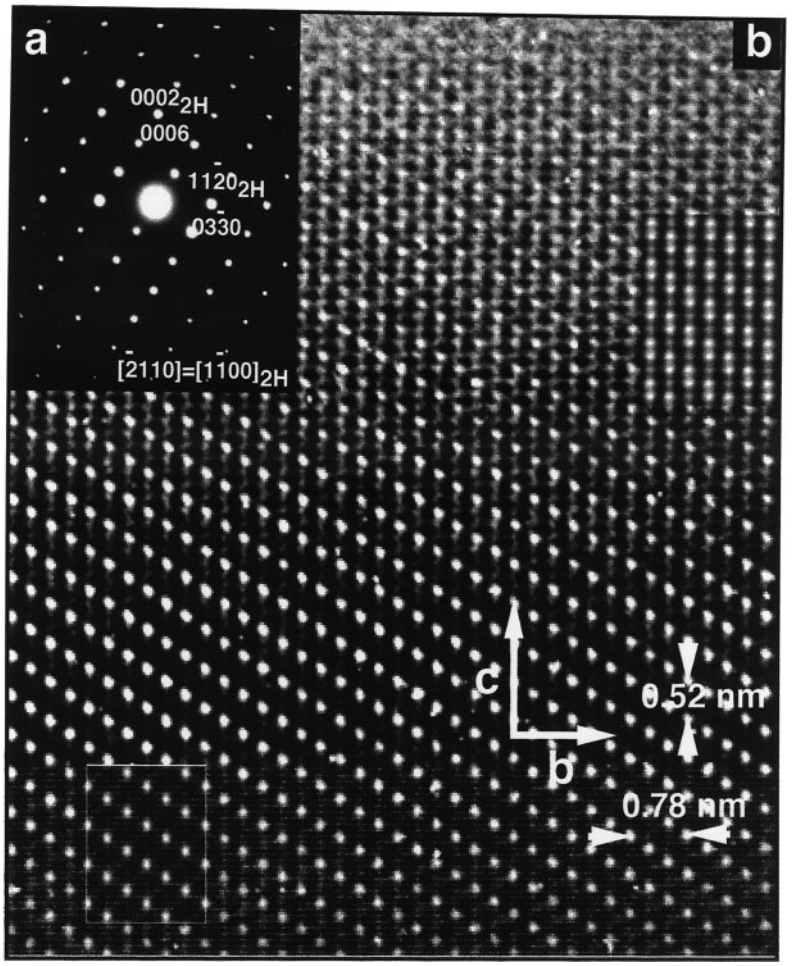

FIG. 8. (a) SAED pattern along $[1\bar{1}00]_{2H}$ corresponding to $Ca_3Co_2O_6$. (b) Corresponding HREM image. The calculated images are shown at the inset.

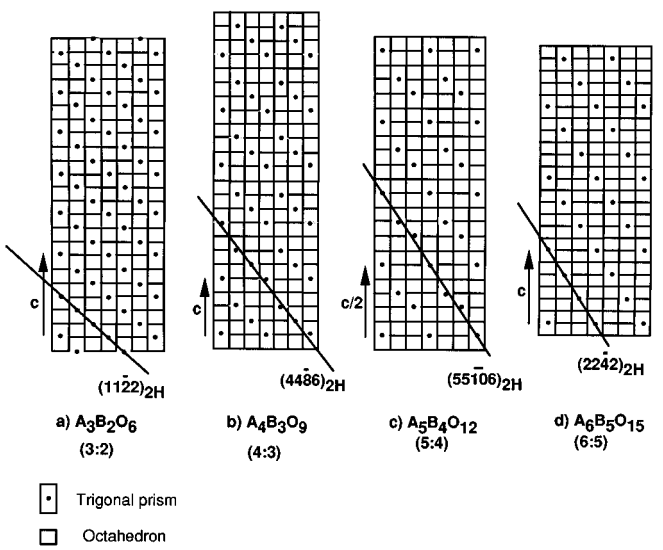

FIG. 9. Idealized representation of (a) (3:2), (b) (4:3), (c) (5:4), and (d) (6:5) structural models along $[1\bar{1}00]_{2H}$. Planes $(11\bar{2}2)_{2H}$, $(44\bar{8}6)_{2H}$, $(55\bar{1}06)_{2H}$, and $(22\bar{4}2)_{2H}$ are outlined.

for the 2H-type, where no superlattice is observed. Such a superstructure is modulated and the z component of the modulation vector decreases as the difference between c_{2H} and c_{Co} decreases down to 0 for the 2H type.

ACKNOWLEDGMENTS

We acknowledge the financial support of CICYT (Spain) through Research Projects MAT95-0642 and MAT98-0648.

REFERENCES

1. D. A. Wadsley, *in* "Nonstoichiometric Compounds" (L. Mandelcorn, Ed.), Chap. 3, p. 135. Academic Press, New York, 1964.
2. E. F. Bertaut, P. Blum, and A. Sagnieres, *Acta Crystallogr.* **12,** 149 (1959).
3. H. D. Megaw, *Proc. Phys. Soc.* **58**(2), 133 (1946).
4. J. C. Grenier, M. Pouchard, and P. Hagenmuller, *Struct. Bonding* **47,** 1 (1981).
5. J. M. González-Calbet and M. Vallet-Regí, *J. Solid State Chem.* **68,** 266 (1987).

6. J. Darriet and M. A. Subramanian, *J. Mater. Chem.* **5,** 543 (1995).
7. J. J. Lander, *Acta Crystallogr.* **4,** 148 (1951).
8. J. J. Randall and L. Katz, *Acta Crystallogr.* **12,** 519 (1959).
9. J. A. Campá, E. Gutiérrez-Puebla, M. A. Monge, I. Rasines, and C. Ruiz-Valero, *J. Solid State Chem.* **108,** 230 (1994).
10. M. Huvé, C. Renard, F. Abraham, G. van Tendeloo, and S. Amelinckx, *J. Solid State Chem.* **135,** 1 (1998).
11. K. Boulahya, M. Parras, and J. M. González-Calbet, *J. Solid State Chem.* **142,** 419 (1999).
12. G. R. Blake, J. Sloan, J. F. Vente, and P. D. Battle, *Chem. Mater.* **10,** 3536 (1998).
13. H. Taguchi, Y. Takeda, F. Kanamara, M. Shimada, and M. Kaizumi, *Acta Crystallogr. B* **33,** 1299 (1977).
14. H. Fjellvag, E. Gulbrandsen, S. Aasland, A. Olsen, and B. C. Hauback, *J. Solid State Chem.* **124,** 190 (1996).
15. W. T. A. Harrison, S. L. Hagwood, and A. J. Jacobson, *J. Chem. Soc., Chem. Commun.* 1953 (1995).
16. R. Christoffersen, A. J. Jacobson, S. L. Hegwood, and L. Liu, *Mater. Res. Soc. Symp. Proc.* **453,** 153 (1997).
17. R. D. Shannon, *Acta Crystallogr. A* **32,** 751 (1976).
18. K. Ukei, A. Yamamoto, Y. Watanabe, T. Shishido, and T. Fukuda, *Acta Crystallogr. B* **49,** 67 (1993).